Steel and Composite Structures, Vol. 1, No. 2 (2001) 245-268
DOI: http://dx.doi.org/10.12989/scs.2001.1.2.245

Analytical evaluation of the moment-rotation response of beam-to-column composite joints under static loading

L. Simões da Silva†

Departamento de Engenharia Civil, Universidade de Coimbra
Polo II, Pinhal de Marrocos, 3030 Coimbra, Portugal

Ana M. Girão Coelho‡

Departamento de Engenharia Civil, Instituto Superior de Engenharia de Coimbra
Quinta da Nora, Apartado 10057, 3031-601 Coimbra, Portugal

Rui A.D. Simões‡†

Departamento de Engenharia Civil, Universidade de Coimbra
Polo II, Pinhal de Marrocos, 3030 Coimbra, Portugal

Abstract. The analysis of steel-concrete composite joints presents some particular aspects that increase their complexity when compared to bare steel joints. In particular, the influence of slab reinforcement and column concrete encasement clearly change the moment-rotation response of the joint. Starting from an energy approach developed in the context of steel joints, an extension to composite joints is presented in this paper that is able to provide closed-form analytical solutions. In addition, the possibility of tri-linear or non-linear component behaviour is also incorporated in the model, enabling adequate treatment of the influence of cracked concrete in tension and the softening response of the column web in compression. This methodology is validated through comparison with experimental tests carried out at the University of Coimbra.

Key words: component method; composite joints; moment resistance; stiffness; non-linear equivalent elastic models.

1. Introduction

Beam-to-column composite joints consist of structural steelwork connections, a continuous reinforced slab and the column web panel. The influence of the slab on the steelwork connections and its interaction with the beam and the column increase the complexity of the analysis of these joints over the simple case of bare steel joints. According to Zandonini (1989), the moment-rotation (M-ϕ) response of a composite joint results from a multitude of phenomena, which include: (i) type of

†Associate Professor
‡Research Assistant
‡†Assistant Professor

connecting elements, (ii) connection configuration, (iii) slippage of bolts, (iv) shear deformation and resistance capacity of the web panel zone, (v) presence of column encasement, (vi) amount, distribution and yield strength of the steel reinforcement, (vii) effect of concrete in tension and (viii) longitudinal interface slip between the steel beam and the concrete slab. For the purpose of simplicity, any joint can be subdivided into three different zones: tension, compression and shear. Within each zone, several sources of deformability can be identified, which are simple elemental parts (or "components") that contribute to the overall response of the joint. This methodology constitutes the basis of the component method (Anderson 1997), currently adopted as the practical approach for predicting the behaviour of steel and composite joints.

Because of the non-linear behaviour of the various components (Silva *et al.* 2001), the evaluation of the M-ϕ response of steel or composite joints requires an incremental non-linear finite element procedure. This approach has been successfully explored by Huber (1999), who developed a computer program to evaluate the M-ϕ response of composite joints. To overcome this complexity, the methodology developed for bare steel joints (Silva *et al.* 2000) is extended in this paper to accommodate composite joints. More specifically, the analytical approach presented below is applied to the analysis of beam-to-column composite joints subjected to hogging moment. It incorporates the effect of the slab (concrete and steel reinforcement), further allowing for non-linear component behaviour. Closed-form solutions are derived that define the full non-linear M-ϕ response, thus enabling characterisation of the usual three properties: initial rotational stiffness, resistance and rotation capacity. Finally, the procedure is validated through comparison with available experimental data.

2. Six-degree-of-freedom non-linear model for the analysis of beam-to-column composite joints

2.1. General remarks

The proposed analytical approach for the analysis of composite joints relies on the component method (Anderson 1997). The essence of this method is that the overall response of a joint may be determined from the mechanical properties of its deformable parts (components), as already pointed out. In the particular case of Fig 1a, illustrating a bolted flush end-plate beam-to-column composite

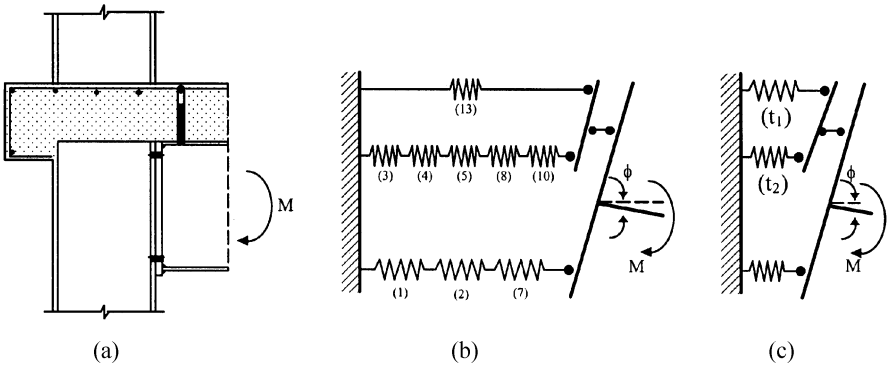

Fig. 1 Proposed analytical procedure for the analysis of a composite joint in bending. (a) Bolted flush end-plate beam-to-column composite connection, (b) Mechanical model, and (c) Equivalent abridged model

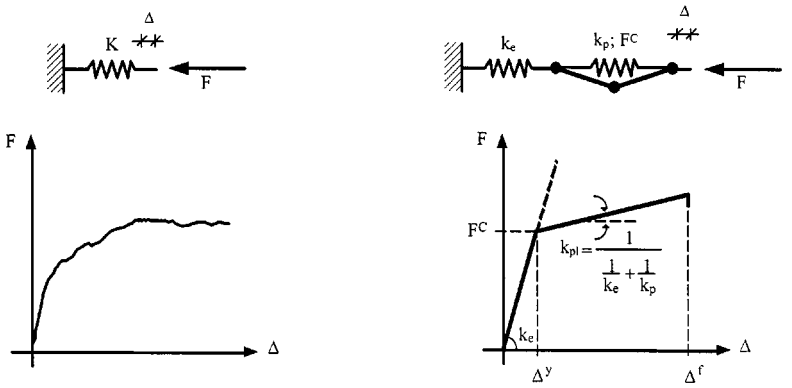

Fig. 2 Equivalent elastic model for a spring in compression: Bi-linearity for modelling elastic-plasticity

connection in bending, the relevant components are: column web panel in shear (1), column web in compression (2), column web in tension (3), column flange in bending (4), end-plate in bending (5), beam flange and web in compression (7), beam web in tension (8), bolts in tension (10) and longitudinal slab reinforcement in tension (13) (Eurocode 4 1999). Each component is characterised by a non-linear force-deformation (F-Δ) response, which can be approximated by simpler curves (Silva and Coelho 2000). These individual components are assembled into a mechanical model, made up of rigid links and extensional springs, in order to evaluate the M-ϕ response of the whole joint Fig. 1b. The spring model of Fig. 1b can be simplified by replacing each assembly of spring in series by an equivalent elastic-plastic spring, which retains all the relevant characteristics Fig. 1c. Several alternative spring and rigid link models have been proposed (Huber and Tschemmernegg 1998), which share the same basic components but basically introduce explicitely the effect of the finite depth of the column.

By means of an elastic analogy of elastic-plastic behaviour, each non-linear spring from the abridged model of Fig. 1c can be replaced by an equivalent elastic system consisting of a set of elastic springs. Fig. 2 shows the particular case of a bi-linear approximation to the actual F-Δ curve for a spring in compression (Silva *et al.* 2000a). For the replacement elastic system, four properties must be specified: elastic stiffness (k_e), post-limit stiffness ($k_{pl} = 1/(1/k_e + 1/k_p)$) , resistance ($F^C$) and collapse deformation (Δ^f). Using this simplification, a general non-linear equivalent elastic model for the analysis of beam-to-column composite joints is presented below.

2.2. Six-degree-of-freedom equivalent elastic model

Consider the six-degree-of-freedom equivalent elastic model (*BL-BL-BL*) of Fig. 3, whereby the component springs exhibit the bi-linear F-Δ response typified in Fig. 2. The degrees-of-freedom are defined as follows:

q_1 - total rotation of the joint ($q_1 = \phi$);
q_2 - rotation of rigid links (length L_c) in compression zone (index c);
q_{3i} - rotation of rigid links (length L_{t_i}) in tension zone (index t), $i = 1, 2$;
q_4 - axial displacement of the joint;

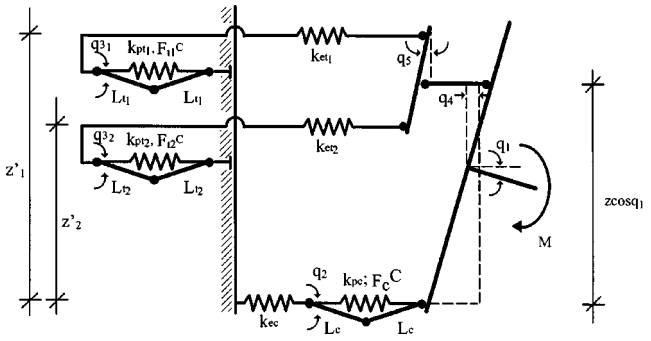

Fig. 3 Six-degree-of-freedom equivalent elastic model for the analysis of beam-to-column composite joints

q_5 - rotation of the tensile zone of the joint;

Using an energy formulation, the following total potential energy function is obtained:

$$V(q_1,q_2,q_3,q_4,q_5)=\frac{1}{2}k_{ec}\left[q_4+\frac{z}{2}\sin q_1-2L_c(1-\cos q_2)\right]^2$$

$$+\frac{1}{2}k_{et_1}\left[q_4-z_1\sin q_5+z\left(\sin q_5-\frac{\sin q_1}{2}\right)+2L_{t_1}(1-\cos q_{3_1})\right]^2$$

$$+\frac{1}{2}k_{et_2}\left[q_4-z_2\sin q_5+z\left(\sin q_5-\frac{\sin q_1}{2}\right)+2L_{t_2}(1-\cos q_{3_2})\right]^2$$

$$+\frac{1}{2}k_{pc}\left[\frac{F_c^C}{k_{pc}}+2L_c(1-\cos q_2)\right]^2+\frac{1}{2}k_{pt_1}\left[\frac{F_{t1}^C}{k_{pt_1}}+2L_{t_1}(1-\cos q_{3_1})\right]^2+\frac{1}{2}k_{pt_2}\left[\frac{F_{t2}^C}{k_{pt_2}}+2L_{t_2}(1-\cos q_{3_2})\right]^2-Mq_1 \qquad (1)$$

where F^C represents the limit load of the component, applied as a pre-compression. The equilibrium paths reproduced in Annex I are determined by differentiating the above function with respect to the various degrees-of-freedom (q_i), setting $\partial V/\partial q_i=0$ and solving the resulting system of equations.

3. Application to bolted flush end-plate beam-to-column composite joints

In order to illustrate the application of the proposed model (*BL-BL-BL*), two joint configurations were selected, corresponding to single-sided (E3 and E5) and double-sided (E1 and E7) bolted flush end-plate beam-to-column composite joints. These were tested in bending by Simões (2000) at the University of Coimbra (Figs. 4 and 5) based on previous experimental work on composite joints (Anderson and Najafi 1994, Li *et al*. 1996). For all test arrangements, the beam consists of an IPE 270 section, rigidly connected to a reinforced concrete slab (full interaction) by eight shear block connectors. The slab, 900 mm wide and 120 mm thick, is reinforced with 10 ∅12 longitudinal bars and 10 ∅8 transversal bars per meter, with 20 mm cover. The steel connection includes a 12 mm thick flush end-plate, welded to the beam and bolted to the column flange with preloaded M20 grade 8.8 bolts. The

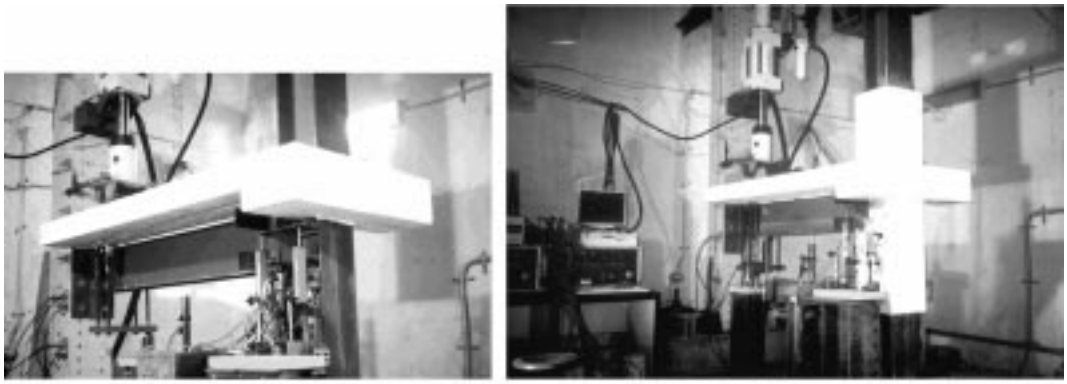

Fig. 4 Single-sided beam-to-column composite joints. (a) Specimen E3 Steel Column, and (b) Specimen E5 Composite Column

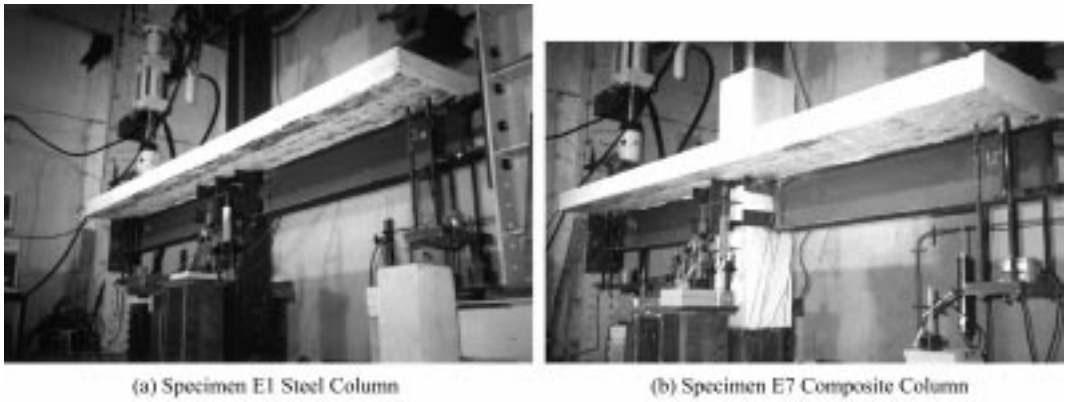

Fig. 5 Double-sided beam-to-column composite joints. (a) Specimen E1 Steel Column, and (b) Specimen E7 Composite Column

column steel section used in all tests was HEA 220 and is totally encased in concrete (300×300 mm^2) in tests E5 and E7, with longitudinal reinforcement of 4 ∅12 (one bar in each corner of the section) and ∅6 bar stirrups, 80 mm apart. The materials employed were: S235 for the steel members, high yield bars for the steel reinforcement and concrete strength class C35/45 for the slab member and column encasement. All the steel and concrete coupon test results are given in Table 1.

The experimental results are compared with the analytical results and the code predictions of Eurocode 4 (1999), in terms of the overall M-ϕ curves and, in particular, moment resistance, taken as the maximum moment ($M_{\max}$), and initial stiffness ($S_{j.ini}$) of the joints.

3.1. Single-sided composite joints (E3 and E5)

Assuming a bi-linear approximation to the F-Δ response of each component, four properties must be characterised: k_e, k_{pl}, F^C and Δ^f, as already shown in Fig. 2b. Both resistance and elastic stiffness for the joint components are determined according to the analytical formulae presented in Eurocode 4 (1999),

Table 1 Mechanical properties of joint materials

Steel specimens			Yield strength (MPa)	Ultimate strength (MPa)	Yield strain (%)	Ultimate strain (%)	Youngs modulus (GPa)
Batch 1	Beam (IPE270)	Web	306	439	23.9	31.8	198
		Flange	267	415	24.4	36.1	203
	Column (HEA220)	Web	328	476	22.1	31.5	198
		Flange	303	459	20.6	34.5	211
	End-plate		283	437	23.7	31.0	206
	Bolts			939			219
Batch 2	Beam (IPE270)	Web	345	508	21.3	31.8	203
		Flange	311	493	20.9	34.9	208
	Column (HEA220)	Web	495	589	17.5	25.6	204
		Flange	479	578	13.9	21.2	213
	End-plate		304	460	23.7	36.6	217
	Bolts			1008			209
Connectors			376	645	17.1	33.3	175
Rebars	∅ 6		470	614	13.6	17.6	208
	∅ 8		513	600	16.4	23.2	212
	∅ 12		541	639	15.0	25.6	205

Concrete specimens	Unit weight	Mean cylinder compressive strength (MPa)	Young's modulus (GPa)
E1 (23 days)	2.32	27.65	31.3
E3 (16 days)	2.37	39.00	34.3
E5 (16 days)	2.37	28.90	31.6
E7 (34 days)	2.35	29.57	31.8

assuming unit values for the partial safety coefficients and using the material data from the experiments. To quantify the post-limit stiffness, some trial values are assumed for equivalent stiffness k_p, based on the available experimental M-ϕ curves, since code regulations do not cover this specific property and very few results currently exist concerning the characterisation of components until failure (Kuhlmann *et al*. 1998). Also, no ductility limits are imposed on each component due to lack of data. The collapse deformation of the components, Δ_i^f, does not need to be introduced in the equations but is used instead to establish failure by checking the following inequality: $\Delta_i \leq \Delta_i^f$. The relevance of establishing actual values for Δ_i^f is greatly reduced by using the three component ductility classes proposed in the literature (Kuhlmann *et al*. 1998):

(i) components with high ductility, not imposing any bounds on the F-Δ response, $(\Delta_i^f/\Delta_i^y = \infty)$;

(ii) components with limited ductility $(1 < \Delta_i^f/\Delta_i^y = \infty)$, which require a value for Δ_i^f; according to Silva *et al*. (2001), the Δ_i^f/Δ_i^y values for components with limited ductility should take values between 2 and 5 for most components;

(iii) brittle components $(\Delta_i^f/\Delta_i^y = 1)$.

Tables 2 and 3 summarize the component characteristics for specimens E3 and E5, respectively. It should be noted that for the longitudinal slab reinforcement in tension the elastic stiffness coefficient is obtained from the proposed method by Ahmed and Nethercot (1997). The influence of the slip between steel and concrete is excluded from the derivation of joint stiffness because there is no guidance for the

Table 2 Component properties for specimen E3

Component		F^C (kN)	k_e (kN/m)	k_p (kN/m)	k_{pl} (kN/m)	Δ^y (mm)
1	Column web panel in shear	394.60	500 940	10 000	9 804	0.788
2	Column web in compression	301.68	1 310 760	4 500	4 485	0.230
3	Column web in tension	283.60	898 920	10	10	0.315
4	Column flange in bending	209.89	2 679 700	10 000	9 963	0.078
5	End-plate in bending	256.10	1 979 660	10 000	9 950	0.129
7	Beam flange and web in compression	495.13	∞	0	0	0.000
8	Beam web in tension	399.25	∞	0	0	0.000
10	Bolts in tension	414.10	2 409 000	10 000	9 956	0.172
13	Longitudinal slab reinforcement in tension	229.46	475 600	10	10	0.482

Table 3 Component properties for specimen E5

Component		F^C (kN)	k_e (kN/m)	k_p (kN/m)	k_{pl} (kN/m)	Δ^y (mm)
1	Column web panel in shear	806.30	799 680	27 000	26 118	1.008
2	Column web in compression	1319.70	3 100 800	10	10	0.426
3	Column web in tension	424.00	891 480	10	10	0.476
4	Column flange in bending	319.30	2 534 700	10 000	9 961	0.126
5	End-plate in bending	293.70	2 321 900	10 000	9 957	0.126
7	Beam flange and web in compression	578.50	∞	39 000	39 000	0.000
8	Beam web in tension	462.10	∞	0	0	0.000
10	Bolts in tension	444.53	2 299 000	10 000	9 957	0.193
13	Longitudinal slab reinforcement in tension	458.93	471 500	10	10	0.973

calculation of the deformation of block shear connectors (Simões 2000). Since these type of connectors are very stiff when compared to other types, its deformation is very small.

Using the appropriate transformation criterion for assemblies of springs in series (Silva and Coelho 2001), the equivalent components are fully defined. Their properties are summed up in Table 4 for both specimens E3 and E5. Fig. 6 reproduces the M-ϕ response of joint E3, comparing the experimental results with the Eurocode 4 predictions and the analytical solutions. Clearly, a good agreement is shown between the three procedures, giving similar results in terms of maximum moment and initial stiffness (Table 5).

The equivalent elastic model enables identification of the critical components and the corresponding bifurcation points in the M-ϕ curve. For joint E3 the model pinpoints the component "column web in compression" as the first critical component ($M = 93.62$ kNm; $\phi = 3.84$ mrad), as confirmed by the experimental observations (Simões 2000). The yielding of the reinforcing bars closer to the column and the cracking of concrete contributed to the failure mode as well, as asserted by the analytical model ($M = 108.46$ kNm; $\phi = 38.43$ mrad).

For joint E5, the experimental M-ϕ curve is plotted alongside with the analytical solutions and the Eurocode 4 predictions in Fig. 7. Table 5 compares the resistance and the initial stiffness of this joint. Again, a fine correlation between the different approaches is observed. The failure mode of joint E5 is due to the yielding of the lower zone of the beam web and flange and the reinforcing bars (Simões 2000). The analytical model identifies this sequence of failure, as expected: the component "beam

Table 4 Data used in the analytical model for specimens E3 and E5

		Equivalent compressive spring	Equivalent tensile springs	
			Row 1	Row 2
Joint **E3**	k_e (kN/m)	3.62×10^5	4.76×10^5	4.16×10^5
	k_p (kN/m)	4.56×10^3	1.00×10^1	7.28×10^3
	P^B (kN)	603.40	458.93	419.78
	L (m)	1.00	1.00	1.00
	z_i (m)		0.36	0.22
	$z = \dfrac{k_{et_1}z_1^2 + k_{et_2}z_2^2}{k_{et_1}z_1 + k_{et_2}z_2} = 0.31$ m			
Joint **E5**	k_e (kN/m)	6.36×10^5	4.72×10^5	4.20×10^5
	k_p (kN/m)	3.90×10^4	1.00×10^1	5.54×10^3
	P^B (kN)	1157.00	917.85	587.40
	L (m)	1.00	1.00	1.00
	z_i (m)		0.36	0.22
	$z = \dfrac{k_{et_1}z_1^2 + k_{et_2}z_2^2}{k_{et_1}z_1 + k_{et_2}z_2} = 0.31$ m			

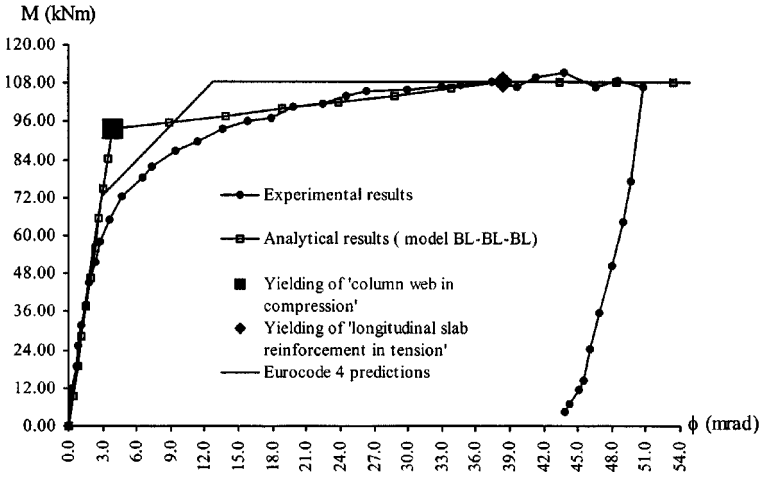

Fig. 6 Moment-rotation curves for joint E3: comparison between experimental results, analytical *BL-BL-BL* model and Eurocode 4 predictions

flange and web in compression" yields at ($M = 178.89$ kNm; $\phi = 5.17$ mrad) and the "longitudinal slab reinforcement in tension" yields at ($M = 217.46$ kNm; $\phi = 16.69$ mrad).

3.2. Double-sided composite joints (E1 and E7)

Tables 6 and 7 show the component properties for specimens E1 and E7, respectively, determined as above. The properties of the equivalent springs to be inserted in the equivalent elastic model are obtained through replacement of the spring assembly in series, by choosing the adequate transformation criterion (Silva and Coelho 2001). These properties are reproduced in Table 8 for joints E1 and joint E7.

Table 5 Moment resistance and initial stiffness of joints E3 and E5

		Experimental results	Analytical results	Eurocode 4 predictions
Joint **E3**	M_{max} (kNm)	111.330 (ϕ = 43.91 mrad)	108.46 (ϕ = 38.43 mrad)	108.56
	$S_{j.ini}$ (kNm/mrad)	27.00	24.39	25.31
Joint **E5**	M_{max} (kNm)	217.60 (ϕ = 20.41 mrad)	217.46 (ϕ = 16.69 mrad)	189.76
	$S_{j.ini}$ (kNm/mrad)	43.10	34.57	35.41

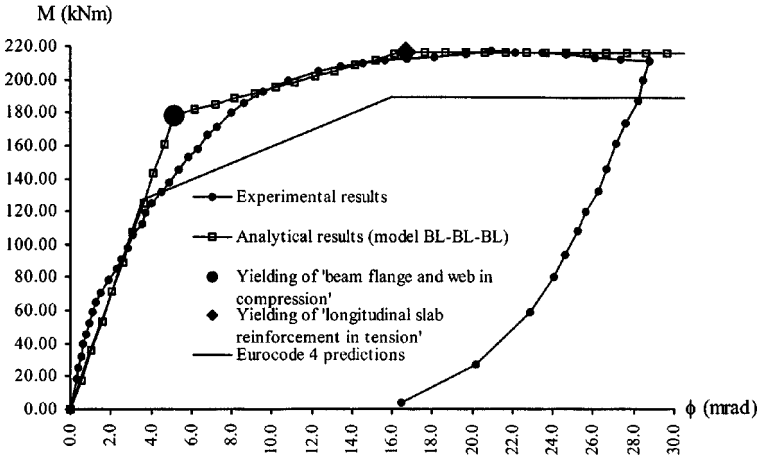

Fig. 7 Moment-rotation curves for joint E5: comparison between experimental results, analytical *BL-BL-BL* model and Eurocode 4 predictions

The M-ϕ response of joint E1 is plotted in Fig. 8 for the three approaches mentioned above. Some disparity is evident, in particular in the post-limit behaviour of the joint. Such discrepancy possibly arises from the insufficient characterisation of the critical component "column web in compression". The analytical model pinpoints the instability of this component at (M = 124.38 kNm; ϕ = 2.22 mrad) but does not account for its highly unstable non-linear behaviour. Table 9 summarises the values of maximum moment and initial stiffness of joint E1, highlighting, again, the differences stated earlier.

For joint E7, Fig. 9 indicates some inconsistency between the experimental results, the analytical predictions of Eurocode 4 and the equivalent elastic model. These differences arise in the lower part of

Table 6 Component properties for specimen E1

Component		F^C (kN)	k_e (kN/m)	k_p (kN/m)	k_{pl} (kN/m)	Δ^y (mm)
2	Column web in compression	391.27	1 314 720	10	10	0.298
3	Column web in tension	326.40	906 840	10	10	0.360
4	Column flange in bending	198.07	2 468 700	10 000	9 960	0.080
5	End-plate in bending	256.10	1 985 840	10 000	9 950	0.129
7	Beam flange and web in compression	495.32	∞	0	0	0.000
8	Beam web in tension	404.55	∞	0	0	0.000
10	Bolts in tension	414.10	2 430 900	10 000	9 959	0.170
13	Longitudinal slab reinforcement in tension	611.90	602 700	10	10	1.015

Table 7 Component properties for specimen E7

Component		F^C (kN)	k_e (kN/m)	k_p (kN/m)	k_{pl} (kN/m)	Δ^y (mm)
2	Column web in compression	1550.20	3 243 600	10	10	0.478
3	Column web in tension	504.00	940 440	10	10	0.536
4	Column flange in bending	346.20	2 982 000	10 000	9 967	0.116
5	End-plate in bending	293.70	2 321 900	10 000	9 957	0.126
7	Beam flange and web in compression	578.50	∞	36 000	36 000	0.000
8	Beam web in tension	462.10	∞	0	0	0.000
10	Bolts in tension	444.53	2 257 200	10 000	9 956	0.197
13	Longitudinal slab reinforcement in tension	477.28	600 650	1 200	1 198	0.795

Table 8 Data used in the analytical model for specimens E1 and E7

		Equivalent compressive spring	Equivalent tensile springs	
			Row 1	Row 2
Joint **E1**	k_e (kN/m)	1.31×10^6	6.03×10^5	4.13×10^5
	k_p (kN/m)	1.00×10^1	1.00×10^1	6.46×10^3
	P^B (kN)	782.60	1223.80	396.14
	L (m)	1.00	1.00	1.00
	z_i (m)		0.36	0.22
	$z = \dfrac{k_{et_1} z_1^2 + k_{et_2} z_2^2}{k_{et_1} z_1 + k_{et_2} z_2} = 0.32$ m			
Joint **E7**	k_e (kN/m)	3.24×10^6	6.01×10^5	4.40×10^5
	k_p (kN/m)	3.60×10^4	1.20×10^3	6.05×10^3
	P^B (kN)	1157.00	954.56	587.40
	L (m)	1.00	1.00	1.00
	z_i (m)		0.36	0.22
	$z = \dfrac{k_{et_1} z_1^2 + k_{et_2} z_2^2}{k_{et_1} z_1 + k_{et_2} z_2} = 0.32$ m			

the curve, although a good agreement is obtained in terms of maximum moment and initial stiffness of the joint, as also seen in Table 9. The yielding sequence of the critical components is: “beam flange and web in compression” and “longitudinal slab reinforcement in tension”, the corresponding critical points in the analytical M-ϕ curve being: (M=182.36 kNm; ϕ=3.46 mrad) and (M=216.47 kNm; ϕ=12.42 mrad), respectively.

3.3. Discussion

Analysis of the experimental M-ϕ characteristics for the four test arrangements clearly shows the loss of stiffness for low values of bending moment. This tendency is even more marked in the joints with concrete encasement (E5 and E7). According to the experimental observations, this loss of stiffness may result from the effect of the “concrete in tension”. Currently, the component “longitudinal slab reinforcement in tension” does not account for cracking of concrete (Ahmed and Nethercot 1997), leading to the divergent results shown in Figs. 6-9.

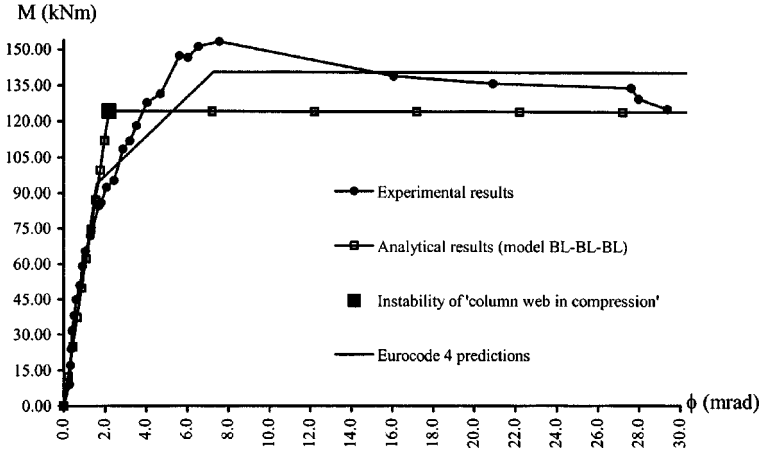

Fig. 8 Moment-rotation curves for joint E1: comparison between experimental results, analytical *BL-BL-BL* model and Eurocode 4 predictions

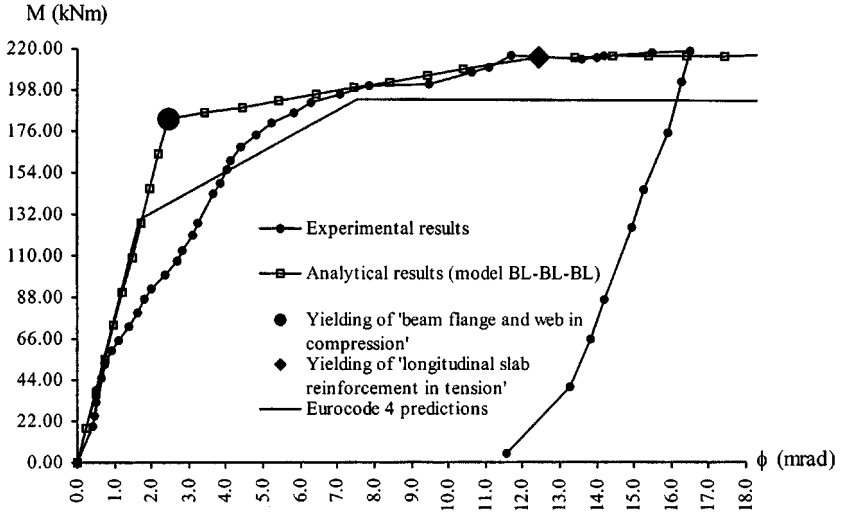

Fig. 9 Moment-rotation curves for joint E7: comparison between experimental results, analytical BL-BL-BL model and Eurocode 4 predictions

Also, whenever the critical component involves loss of stability, e.g., “column web in compression”, the behaviour of such components usually presents a limit point and a subsequent softening response,

Table 9 Moment resistance and initial stiffness of joints E1 and E7

		Experimental results	Analytical results	Eurocode 4 predictions
Joint **E3**	M_{max} (kNm)	153.59 (ϕ=7.58 mrad)	124.39 (ϕ=7.22 mrad)	140.78
	$S_{j.ini}$ (kNm/mrad)	62.50	56.14	57.76
Joint **E5**	M_{max} (kNm)	219.82(ϕ=16.53 mrad)	217.38(ϕ=16.42 mrad)	193.68
	$S_{j.ini}$ (kNm/mrad)	81.30	75.06	76.69

not adequately reproduced by a bi-linear representation. Such behaviour influences the rotational response of the whole joint, resulting in a further departure from a linear M-ϕ curve, as shown in Fig. 8.

To overcome both these problems, a general seven-degree-of-freedom model catering for multi-linear and non-linear component characterisation is developed below.

4. Seven-degree-of-freedom non-linear model for the analysis of beam-to-column composite joints

4.1. Seven-degree-of-freedom equivalent elastic model

The analytical methodology can be extended to include the effects of the concrete in tension and the non-linear behaviour of the component "column web in compression". To allow for the stiffness reduction due to the cracking of concrete an extra-degree-of-freedom is brought in within the upper component in tension in the previous model (*BL-BL-BL*). The resulting seven-degree-of-freedom model (*NL-BL-TL*) is illustrated in Fig. 10. This model also accomodates post-yield non-linear behaviour in the compressive zone. According to Silva and Coelho (2000) the equivalent post-limit stiffness is written as a quadratic polynomial function of $(1-\cos q_2)$:

$$k_{pc} = k_{pc1} + 4L_c k_{pc2}(1-\cos q_2) + 12L_c^2 k_{pc3}(1-\cos q_2)^2 \tag{2}$$

where k_{pc1}, k_{pc2} and k_{pc3} are general stiffness coefficients. The resulting total potential function is given by:

$$V(q_1, q_2, q_{3_{1,1}}, q_{3_{1,2}}, q_{3_2}, q_4, q_5) = \frac{1}{2}k_{ec}\left[q_4 + \frac{z}{2}\sin q_1 - 2L_c(1-\cos q_2)\right]^2$$

$$+\frac{1}{2}k_{et_1}\left[q_4 - z_1\sin q_5 + z\left(\sin q_5 - \frac{\sin q_1}{2}\right) + 2L_{t_{1,1}}(1-\cos q_{3_{1,1}}) + 2L_{t_{1,2}}(1-\cos q_{3_{1,2}})\right]^2$$

$$+\frac{1}{2}k_{et_2}\left[q_4 - z_2\sin q_5 + z\left(\sin q_5 - \frac{\sin q_1}{2}\right) + 2L_{t_2}(1-\cos q_{3_2})\right]^2 + \frac{1}{2}k_{pc1}\left[\frac{F_c^C}{k_{pc1}} + 2L_c(1-\cos q_2)\right]^2$$

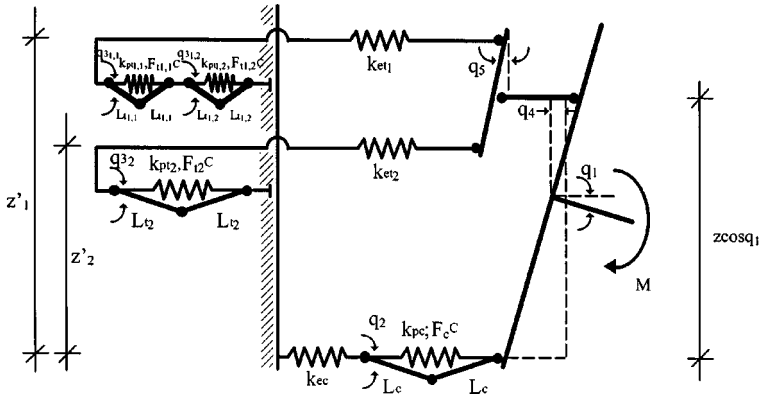

Fig. 10 Seven-degree-of-freedom equivalent elastic model for the analysis of beam-to-column composite joints

$$+\frac{1}{2}k_{pt_{1,1}}\left[\frac{F^{C}_{t1,1}}{k_{pt_{1,1}}}+2L_{t_{1,1}}(1-\cos q_{3_{1,1}})\right]^2+\frac{1}{2}k_{pt_{1,2}}\left[\frac{F^{C}_{t1,2}}{k_{pt_{1,2}}}+2L_{t_{1,2}}(1-\cos q_{3_{1,2}})\right]^2+\frac{1}{2}k_{pt_2}\left[\frac{F^{C}_{t2}}{k_{pt_2}}+2L_{t_2}(1-\cos q_{3_2})\right]^2$$

$$+\frac{1}{3}k_{pc2}[2L_c(1-\cos q_2)]^3+\frac{1}{4}k_{pc3}[2L_c(1-\cos q_2)]^4-Mq_1 \quad (3)$$

Applying the same procedure from above and assuming $F^{C}_{t1,1}<F^{C}_{t1,2}$, the relevant equilibrium paths of the system are obtained Annex II.

4.2. Examples

The application of model *NL-BL-TL* to the previous examples requires the assessment of the cracking force of the concrete in tension and the subsequent characterisation of the component "longitudinal slab reinforcement in tension" using a tri-linear approximation. The *F*-Δ relationship for this "new" component involves three regimes: an elastic range under uncracked slab conditions, an elastic domain under cracked conditions and a non-linear inelastic phase corresponding to the yielding of the reinforcing bars. The first elastic regime is characterised by a value of stiffness k_e, which can be defined in accordance with the analytical formulae from Eurocode 4 (1999). A second elastic regime, under cracked slab conditions, then follows on from the attainment of the cracking force of the concrete in tension with reducing stiffness. To quantify these latter parameters, some random values are tested so that the analytical *M*-ϕ curve best fits to the experimental one. The yielding of the reinforcing bars makes the component enter the inelastic phase as the ultimate resistance capacity is reached. Again, this resistance is determined in accordance with Eurocode 4 (1999) and based on the experimental results.

Also, in order to account for the non-linear unstable response of test specimen E1, the behaviour of the critical component "column web in compression" is reproduced by a cubic approximation to the post-limit *F*-Δ response. The parameters which describe the non-linear post-limit stiffness are adjusted trial values that are able to mimic the *M*-ϕ curve from the experiments.

Table 10 summarises the new component properties for the four examples to be used in conjunction with the seven-degree-of-freedom model. Figs. 11-14 illustrate the analytical *M*-ϕ curves using this new approach, showing perfect agreement with the experiments. Compared to the *BL-BL-BL* model, the *NL-BL-TL* model yields equivalent results in terms of moment resistance and initial stiffness, but shows improved performance in reproducing the actual rotational joint behaviour. For all test arrangements,

Table 10 New data used in the analytical model *NL-BL-TL*

	Single-sided joints		Double-sided joints	
	E3	E5	E1	E7
k_{pc1}(kN/m)	9.12×10^3	7.80×10^4	6.80×10^4	6.48×10^4
k_{pc2}(kN/m^2)	0.00	0.00	-1.38×10^7	0.00
k_{pc3}(kN/m^3)	0.00	0.00	6.80×10^8	0.00
$k_{pt_{1,1}}$(kN/m)	1.70×10^4	1.57×10^5	1.59×10^5	2.31×10^5
$k_{pt_{1,2}}$(kN/m)	1.00×10^1	1.00×10^1	1.00×10^1	1.20×10^3
$P^{B}_{T1,1}$(kN)	282.42	435.02	317.72	249.98
$P^{B}_{T1,2}$(kN)	458.93	917.85	679.21	954.56

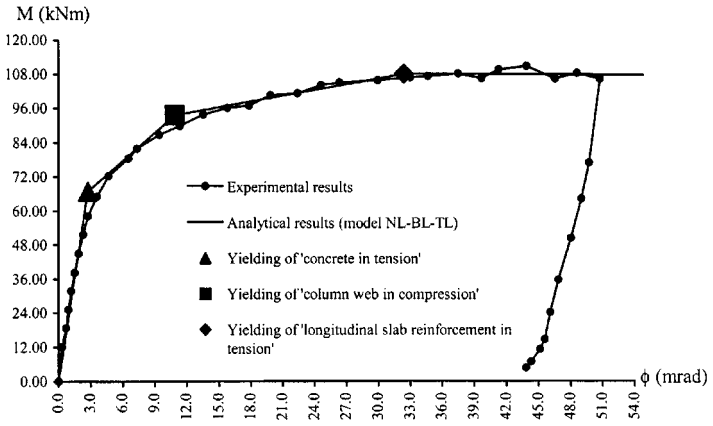

Fig. 11 Moment-rotation curves for joint E3: comparison between experimental results and the *NL-BL-TL* analytical model

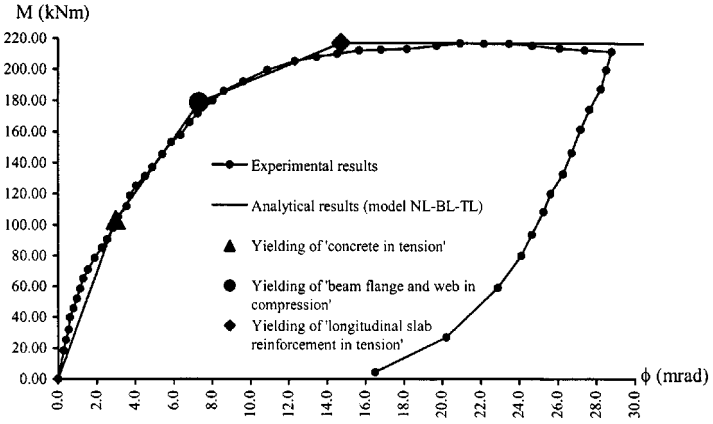

Fig. 12 Moment-rotation curves for joint E5: comparison between experimental results and the *NL-BL-TL* analytical model

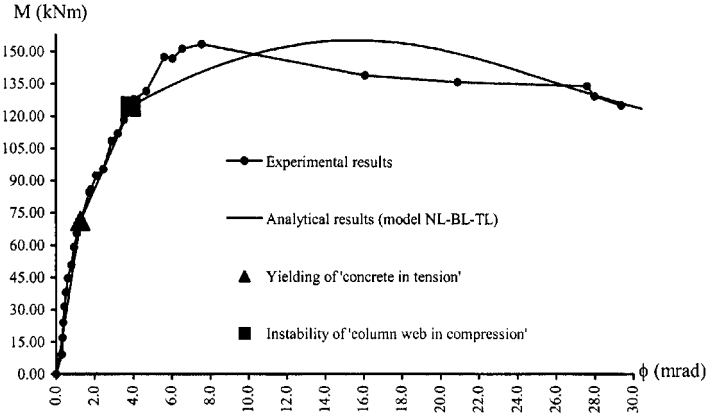

Fig. 13 Moment-rotation curves for joint E1: comparison between experimental results and the *NL-BL-TL* analytical model

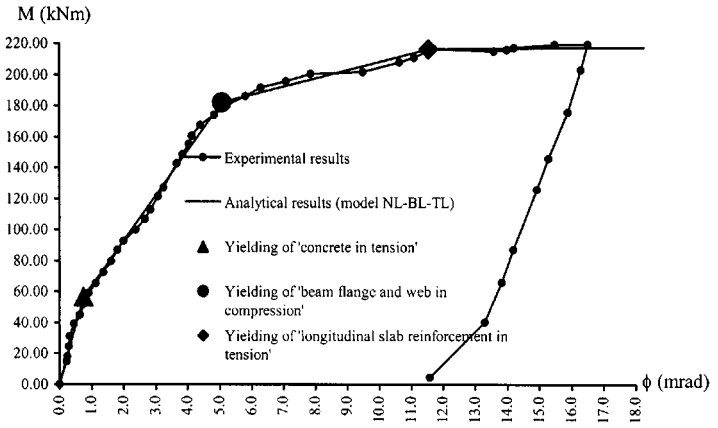

Fig. 14 Moment-rotation curves for joint E7: comparison between experimental results and the *NL-BL-TL* analytical model

the first reduction in stiffness is due to the cracking of concrete. The subsequent component failure sequence remains identical to the previous model and occurs at similar levels of bending moment but at different values of rotation.

It is finally worth noting that the analytical prediction of the behaviour of joint E1 has improved when compared to the earlier approach. Taking the post-limit response of the column web in compression into account, the joint softening response is better represented.

5. Conclusions

An analytical methodology for the prediction of composite beam-to-column joint behaviour has been presented. Recently, a comprehensive procedure for the full analysis of bare steel joint has been developed (Silva and Coelho 2001). In the context of the component method, any joint (steel or composite) can be regarded as a set of components assembled in series and/or parallel. The assessment of composite joint behaviour, however, must account for the concrete slab action in the uncracked and cracked regime, as well as its interaction with the steel/composite members. Therefore, the analysis of such type of joints presents the further difficulty of an additional row of springs, corresponding to the combined response of steel reinforcement and concrete in tension. The need to reproduce adequately the appropriate lever arms z_i in the component model required the development of a model with two rows in tension (*BL-BL-BL*). This gave good results but failed to reproduce effects of the “concrete in tension” and individual component instability over the overall joint behaviour.

Previous shortcomings were solved by a further sophistication, involving non-linear component characterisation (*NL-BL-TL*) (Silva and Coelho 2000) in order to accommodate the imperfection-sensitivity of components exhibiting instability phenomena, and accounting for the slab behaviour under cracked conditions.

Both analytical models yield identical results in terms of resistance and initial rotational stiffness but show different results in relation to the joint ductility, as highlighted by Figs. 6 and 11 for joint

E3, for example. In this particular case, for instance, the "column web in compression" becomes unstable at similar levels of bending moment but at a lower value of rotation, for the simplified model.

Finally, the accuracy of this methodology is highly dependent on the precision of the key parameters that characterise the individual components. So far, there is no quantitative guidance on the evaluation of both post-limit stiffness and collapse deformation of elemental components. As already pointed out, both properties play a very important role in the prediction of joint behaviour, particularly in terms of evaluation of ductility. Current work on this issue is being carried out.

Acknowledgements

Financial support from "Ministério da Ciência e Tecnologia" PRAXIS XXI research project PRAXIS/P/ECM/13153/1998 is gratefully acknowledged.

References

Ahmed B. and Nethercot D.A. (1997), "Prediction of initial stiffness and available rotation capacity of major axis composite endplate connections", *J. Const. Steel Res.*, **41**(1), 31-60.

Anderson D. (ed.) (1997), "Semi-Rigid behaviour of civil engineering structural connections composite steel-concrete joints in braced frames for buildings", COST C1, European Communities, Brussels.

Anderson D. and Najafi A.A. (1994), "Performance of composite connections: major axis end plate joints", *J. Const. Steel Res.*, **31**(1), 31-57.

Eurocode 4, EN 1994-1-1 (1999), "Design of composite steel and concrete structures Part 1.1 (Draft nº1): general rules and rules for buildings", CEN, European Committee for Standardization, Brussels.

Huber G. (1999), "Nicht-lineare berechnungen von verbundquerschnitten und biegeweichen knoten", Ph. D Thesis (in English), University of Innsbruck, Austria.

Huber G. and Tschemmernegg F. (1998), "Modelling of beam-to-column joints", *J. Const. Steel Res.*, **45**, 199-216.

Kulhmann U., Davison J.B., Kattner M. (1998), "Structural systems and rotation capacity", *COST Conference*, Liège, Belgium, September 18-19.

Li T.Q., Nethercot D.A., Choo B.S. (1996), "Behaviour of flush end-plate composite connections with unbalanced moment and variable shear/moment ratios I. Experimental behaviour", *J. Const. Steel Res.*, **38**(2), 125-164.

Silva L.S. and Coelho A.M.G. (2000), "Mode interaction in non-linear models for steel and steel-concrete composite structural connections", In: *Proc. of the Third In. Conf. on Coupled Instabilities in Metal Structures CIMS 2000* (eds.: D. Camotim, D. Dubina and J. Rondal), Imperial College Press, Lisboa, Portugal, 605-614.

Silva L.S., Coelho A.G., Neto E. (2000), "Equivalent post-buckling models for the flexural behaviour of steel connections", *Comp. Struct.*, **77**, 615-624.

Silva L.S. and Coelho A.G. (2001), "A ductility model for steel connections", *J. Const. Steel Res.*, (in print).

Silva L.S., Santiago A., Vila Real P. (2001), "Numerical evalution of the ductility of steel joints", (to be published).

Simões, R.A.D. (2000), "Behaviour of beam-to-column composite joints under static and cyclic loading", Ph. D. Thesis (in portuguese), University of Coimbra, Portugal.

Zandonini R. (1989), "Semi-rigid composite joints", In: *Structural Connections: Stability and Strength* (ed.: R. Narayanan), Elsevier Applied Science, London, 63-120.

Notation

c : Index referring to compression zone
k_e : Elastic stiffness

k_i : Stiffness of component i
k_p : Equivalent post-limit stiffness
k_{pci} : General coefficients to define non-linear equivalent post-limit stiffness
k_{pl} : Post-limit stiffness
q_1 : Total rotation of the joint
q_2 : Rotation of rigid links (compression zone)
$q_{3_{i,j}}$: Rotation of rigid links (tension zone)
q_4 : Axial displacement of the connection
q_5 : Rotation of the tensile zone of the joint
t : Index referring to tension zone
z : Lever arm
z_i : Length of rigid link between tensile component i and the compressive components
z'_i : Vertical projection of z_i
A : Parameter
B : Parameter
C : Parameter
D : Parameter
E : Parameter
F : Force; parameter
F^C : Resistance (limit load) of a component
G : Parameter
H : Parameter
K : Stiffness (general)
L : Length of rigid links
M : Bending moment
$M_{\max}$: Maximum moment reached by a joint
$S_{j.ini}$: Initial stiffness of a joint
V : Total potential energy function
α : Parameter
β : Parameter
χ : Parameter
ϕ : Total rotation of a joint
γ : Parameter
λ : Parameter
μ : Parameter
θ : Parameter
ρ : Parameter
Δ : Total (axial) deformation
Δ_i^f : Collapse deformation
Δ_i^y : Yield deformation

Annex I

(i) Fundamental solution

$$\begin{cases} M = \theta \sin(2q_1) \\ q_2 = 0 = q_{3_1} = q_{3_2} \end{cases} \tag{AI.1}$$

(ii) Uncoupled solution in q_2

$$\begin{cases} M = \theta \sin(2q_1) - \beta_c \cos q_1 (1 - \cos q_2) \\ 1 - \cos q_2 = \dfrac{\beta_c \sin q_1 + 2F_c^C L_c}{2\alpha_c} \\ q_{3_1} = 0 = q_{3_2} \end{cases} \tag{AI.2}$$

(iii) Uncoupled solution in q_{3_1}

$$\begin{cases} M = \theta \sin(2q_1) - \beta_{t_1} \cos q_1 (1 - \cos q_{3_1}) \\ q_2 = 0 = q_{3_2} \\ 1 - \cos q_{3_1} = \dfrac{\beta_{t_1} \sin q_1 - 2F_{t1}^C L_{t_1}}{2\alpha_{t_1}} \end{cases} \tag{AI.3}$$

(iv) Uncoupled solution in q_{3_2}

$$\begin{cases} M = \theta \sin(2q_1) - \beta_{t_2} \cos q_1 (1 - \cos q_{3_2}) \\ q_2 = 0 = q_{3_1} \\ 1 - \cos q_{3_2} = \dfrac{\beta_{t_2} \sin q_1 - 2F_{t2}^C L_{t_2}}{2\alpha_{t_2}} \end{cases} \tag{AI.4}$$

(v) Uncoupled solution in q_2 and q_{3_1}

$$\begin{cases} M = \theta \sin(2q_1) - [\beta_c (1 - \cos q_2) + \beta_{t_1} (1 - \cos q_{3_1})] \cos q_1 \\ 1 - \cos q_2 = \dfrac{(2\alpha_{t_1}\beta_c - \beta_{t_1}\chi_1) \sin q_1 - 4\alpha_{t_1} F_c^C L_c + 2\chi_1 F_{t1}^C L_{t_1}}{4\alpha_c \alpha_{t_1} - \chi_1^2} \\ 1 - \cos q_{3_1} = \dfrac{\beta_{t_1} \sin q_1 - \chi_1 (1 - \cos q_2) - 2F_{t1}^C L_{t_1}}{2\alpha_{t_1}} \\ q_{3_2} = 0 \end{cases} \tag{AI.5}$$

(vi) Uncoupled solution in q_2 and q_{3_2}

$$\begin{cases} M = \theta \sin(2q_1) - [\beta_c (1 - \cos q_2) + \beta_{t_2} (1 - \cos q_{3_2})] \cos q_1 \\ 1 - \cos q_2 = \dfrac{(2\alpha_{t_2}\beta_c - \beta_{t_2}\chi_2) \sin q_1 - 4\alpha_{t_2} F_c^C L_c + 2\chi_2 F_{t2}^C L_{t_2}}{4\alpha_c \alpha_{t_2} - \chi_2^2} \\ q_{3_1} = 0 \\ 1 - \cos q_{3_2} = \dfrac{\beta_{t_2} \sin q_1 - \chi_2 (1 - \cos q_2) - 2F_{t2}^C L_{t_2}}{2\alpha_{t_2}} \end{cases} \tag{AI.6}$$

(vii) Uncoupled solution in q_{3_1} and q_{3_2}

$$\begin{cases} M = \theta\sin(2q_1) - [\beta_{t_1}(1-\cos q_{3_1}) + \beta_{t_2}(1-\cos q_{3_2})]\cos q_1 \\ q_2 = 0 \\ 1-\cos q_{3_1} = \dfrac{\beta_{t_1}\sin q_1 + \chi_3(1-\cos q_{3_2}) - 2F_{t1}^C L_{t_1}}{2\alpha_{t_1}} \\ 1-\cos q_{3_2} = \dfrac{(2\alpha_{t_1}\beta_{t_2} + \beta_{t_1}\chi_3)\sin q_1 - (2\chi_3 F_{t1}^C L_{t_1} - 4\alpha_{t_1} F_{t2}^C L_{t_2})}{4\alpha_{t_1}\alpha_{t_2} - \chi_3^2} \end{cases} \tag{AI.7}$$

(viii) Fully coupled solution in q_2, q_{3_1} and q_{3_2}

$$\begin{cases} M = \theta\sin(2q_1) - [\beta_c(1-\cos q_2) + \beta_{t_1}(1-\cos q_{3_1}) + \beta_{t_2}(1-\cos q_{3_2})]\cos q_1 \\ 1-\cos q_2 = \dfrac{2\alpha_{t_1}}{(4\alpha_c\alpha_{t_1} - \chi_1^2)(4\alpha_{t_1}\alpha_{t_2} - \chi_3^2) - (2\alpha_{t_1}\chi_2 + \chi_1\chi_3)^2}\{[2\alpha_{t_1}(2\alpha_{t_2}\beta_c - \beta_{t_2}\chi_2) \\ \quad -\beta_{t_1}(2\alpha_{t_2}\chi_1 + \chi_2\chi_3) - \chi_3(\beta_c\chi_3 + \beta_{t_2}\chi_1)]\sin q_1 - 2(4\alpha_{t_1}\alpha_{t_2} - \chi_3^2)F_c^C L_c \\ \quad +[2\alpha_{t_2}\chi_1 + \chi_2\chi_3)F_{t1}^C L_{t_1} + 2(2\alpha_{t_1}\chi_2 + \chi_1\chi_3)F_{t2}^C L_{t_2}\} \\ 1-\cos q_{3_1} = \dfrac{\beta_{t_1}\sin q_1 - \chi_1(1-\cos q_2) + \chi_3(1-\cos q_{3_2}) - 2F_{t1}^C L_{t_1}}{2\alpha_{t_1}} \\ 1-\cos q_{3_2} = \dfrac{1}{4\alpha_{t_1}\alpha_{t_2} - \chi_3^2}[(2\alpha_{t_1}\beta_{t_2} + \beta_{t_1}\chi_3)\sin q_1 - (2\alpha_{t_1}\chi_2 + \chi_1\chi_3)\times(1-\cos q_2) - 2\chi_3 F_{t1}^C L_{t_1} - 4\alpha_{t_1} F_{t2}^C L_{t_2}] \end{cases} \tag{AI.8}$$

The parameters in Eqs. (AI.1-8) are defined below.

$$\theta = \frac{z^2(z_1-z_2)^2\rho}{2\lambda} \tag{AI.9}$$

$$\alpha_c = 2L_c^2\left[\frac{(z_1-z_2)^2\rho}{\lambda} + k_{pc}\right] \qquad \beta_c = \frac{2z(z_1-z_2)^2 L_c\rho}{\lambda}$$

$$\alpha_{t_1} = 2L_{t_1}^2\left[\frac{(z_2-z)^2\rho}{\lambda} + k_{pt_1}\right] \qquad \beta_{t_1} = \frac{2z(z_1-z_2)(z_1-z)L_{t_1}\rho}{\lambda}$$

$$\alpha_{t_2} = 2L_{t_2}^2\left[\frac{(z_1-z)^2\rho}{\lambda} + k_{pt_2}\right] \qquad \beta_{t_2} = \frac{2z(z_1-z_2)(z_1-z)L_{t_2}\rho}{\lambda} \tag{AI.10}$$

$$\chi_1 = 4L_c L_{t_1}\frac{(z_1-z_2)(z-z_2)\rho}{\lambda}$$

$$\chi_2 = 4L_c L_{t_2}\frac{(z_1-z_2)(z_1-z)\rho}{\lambda}$$

$$\chi_3 = 4L_{t_1}L_{t_2}\frac{(z_1-z)(z_2-z)\rho}{\lambda} \tag{AI.11}$$

and

$$\lambda = (z-z_1)^2 k_{ec} k_{et_1} + (z-z_2)^2 k_{ec} k_{et_2} + (z_1-z_2)^2 k_{et_1} k_{et_2}$$
$$\rho = k_{ec} k_{et_1} k_{et_2} \tag{AI.12}$$

Annex II

(i) Fundamental solution

$$\begin{cases} M = \theta \sin(2q_1) \\ q_2 = 0 = q_{3_{1,1}} = q_{3_{1,2}} = q_{3_2} \end{cases} \tag{AII.1}$$

(ii) Uncoupled solution in q_2

$$\begin{cases} M = \theta \sin(2q_1) - \beta_c \cos q_1 (1-\cos q_2) \\ 4\mu_c (1-\cos q_2)^3 + 3\gamma_c (1-\cos q_2)^2 + 2\alpha_c (1-\cos q_2) - \beta_c \sin q_1 + 2F_c^C L_c = 0 \\ q_{3_{1,1}} = 0 = q_{3_{1,2}} = q_{3_2} \end{cases} \tag{AII.2}$$

(iii) Uncoupled solution in $q_{3_{1,1}}$

$$\begin{cases} M = \theta \sin(2q_1) - \beta_{t_{1,1}} \cos q_1 (1-\cos q_{3_{1,1}}) \\ q_2 = 0 = q_{3_{1,2}} = q_{3_2} \\ 1-\cos q_{3_{1,1}} = \dfrac{\beta_{t_{1,1}} \sin q_1 - 2F_{t1,1}^C L_{t_{1,1}}}{2\alpha_{t_{1,1}}} \end{cases} \tag{AII.3}$$

(iv) Uncoupled solution in q_{3_2}

$$\begin{cases} M = \theta \sin(2q_1) - \beta_{t_2} \cos q_1 (1-\cos q_{3_2}) \\ q_2 = 0 = q_{3_{1,1}} = q_{3_{1,2}} \\ 1-\cos q_{3_2} = \dfrac{\beta_{t_2} \sin q_1 - 2F_{t2}^C L_{t_2}}{2\alpha_{t_2}} \end{cases} \tag{AII.4}$$

(v) Uncoupled solution in q_2 and $q_{3_{1,1}}$

$$\begin{cases} M = \theta \sin(2q_1) - [\beta_c (1-\cos q_2) + \beta_{t_{1,1}} (1-\cos q_{3_{1,1}})] \cos q_1 \\ A_5 (1-\cos q_2)^3 + B_5 (1-\cos q_2)^2 + C_5 (1-\cos q_2) - D_5 \sin q_1 + E_5 = 0 \\ 1-\cos q_{3_{1,1}} = \dfrac{\beta_{t_{1,1}} \sin q_1 - \chi_{1,1} (1-\cos q_2) - 2F_{t1,1}^C L_{t_{1,1}}}{2\alpha_{t_{1,1}}} \\ q_{3_{1,2}} = 0 = q_{3_2} \end{cases} \tag{AII.5}$$

(vi) Uncoupled solution in q_2 and q_{3_2}

$$\begin{cases} M = \theta\sin(2q_1) - [\beta_c(1-\cos q_2) + \beta_{t_2}(1-\cos q_{3_2})]\cos q_1 \\ A_6(1-\cos q_2)^3 + B_6(1-\cos q_2)^2 + C_6(1-\cos q_2) - D_6\sin q_1 + E_6 = 0 \\ q_{3_{1,1}} = 0 = q_{3_{1,2}} \\ 1-\cos q_{3_2} = \dfrac{\beta_{t_2}\sin q_1 - \chi_2(1-\cos q_2) - 2F_{t2}^C L_{t_2}}{2\alpha_{t_2}} \end{cases} \quad \text{(AII.6)}$$

(vii) Uncoupled solution in $q_{3_{1,1}}$ and $q_{3_{1,2}}$

$$\begin{cases} M = \theta\sin(2q_1) - [\beta_{t_{1,1}}(1-\cos q_{3_{1,1}}) + \beta_{t_{1,2}}(1-\cos q_{3_{1,2}})]\cos q_1 \\ q_2 = 0 = q_{3_2} \\ 1-\cos q_{3_{1,1}} = \dfrac{\beta_{t_{1,1}}\sin q_1 - \chi_4(1-\cos q_{3_{1,2}}) - 2F_{t1,1}^C L_{t_{1,1}}}{2\alpha_{t_{1,1}}} \\ 1-\cos q_{3_{1,2}} = \dfrac{(2\alpha_{t_{1,1}}\beta_{t_{1,2}} - \beta_{t_{1,1}}\chi_4)\sin q_1 - 2\chi_4 F_{t1,1}^C L_{t_{1,1}} - 4\alpha_{t_{1,1}} F_{t1,2}^C L_{t_{1,2}}}{4\alpha_{t_{1,1}}\alpha_{t_{1,2}} - \chi_4^2} \end{cases} \quad \text{(AII.7)}$$

(viii) Uncoupled solution in $q_{3_{1,1}}$ and q_{3_2}

$$\begin{cases} M = \theta\sin(2q_1) - [\beta_{t_{1,1}}(1-\cos q_{3_{1,1}}) + \beta_{t_2}(1-\cos q_{3_2})]\cos q_1 \\ q_2 = 0 = q_{3_{1,2}} \\ 1-\cos q_{3_{1,1}} = \dfrac{\beta_{t_{1,1}}\sin q_1 + \chi_{3,1}(1-\cos q_{3_2}) - 2F_{t1,1}^C L_{t_{1,1}}}{2\alpha_{t_{1,1}}} \\ 1-\cos q_{3_2} = \dfrac{(2\alpha_{t_{1,1}}\beta_{t_2} + \beta_{t_{1,1}}\chi_{3,1})\sin q_1 - 2\chi_{3,1} F_{t1,1}^C L_{t_{1,1}} - 4\alpha_{t_{1,1}} F_{t2}^C L_{t_2}}{4\alpha_{t_{1,1}}\alpha_{t_2} - \chi_{3,1}^2} \end{cases} \quad \text{(AII.8)}$$

(ix) Uncoupled solution in q_2, $q_{3_{1,1}}$ and $q_{3_{1,2}}$

$$\begin{cases} M = \theta\sin(2q_1) - [\beta_c(1-\cos q_2) + \beta_{t_{1,1}}(1-\cos q_{3_{1,1}}) + \beta_{t_{1,2}}(1-\cos q_{3_{1,2}})]\cos q_1 \\ A_9(1-\cos q_2)^3 + B_9(1-\cos q_2)^2 + C_9(1-\cos q_2) - D_9\sin q_1 + E_9 = 0 \\ \\ 1-\cos q_{3_{1,1}} = \dfrac{\beta_{t_{1,1}}\sin q_1 - \chi_{1,1}(1-\cos q_2) - \chi_4(1-\cos q_{3_{1,2}}) - 2F_{t1,1}^C L_{t_{1,1}}}{2\alpha_{t_{1,1}}} \\ 1-\cos q_{3_{1,2}} = \dfrac{1}{4\alpha_{t_{1,1}}\alpha_{t_{1,2}} - \chi_4^2}[(2\alpha_{t_{1,1}}\beta_{t_{1,2}} - \beta_{t_{1,1}}\chi_4)\sin q_1 - (2\alpha_{t_{1,1}}\chi_{1,2} - \chi_{1,1}\chi_4) \\ \qquad \times(\quad - \quad q_2) + 2\chi_4 F_{t1,1}^C L_{t_{1,1}} - 4\alpha_{t_{1,1}} F_{t1,2}^C L_{t_{1,2}}] \qquad 1 \quad \cos \\ q_{3_2} = 0 \end{cases} \quad \text{(AII.9)}$$

(xi) Uncoupled solution in q_2, $q_{3_{1,1}}$ and q_{3_2}

$$\begin{cases} M = \theta\sin(2q_1) - [\beta_c(1-\cos q_2) + \beta_{t_{1,1}}(1-\cos q_{3_{1,1}}) + \beta_{t_2}(1-\cos q_{3_2})]\cos q_1 \\ A_{10}(1-\cos q_2)^3 + B_{10}(1-\cos q_2)^2 + C_{10}(1-\cos q_2) - D_{10}\sin q_1 + E_{10} = 0 \\ 1-\cos q_{3_{1,1}} = \dfrac{\beta_{t_{1,1}}\sin q_1 - \chi_{1,1}(1-\cos q_2) + \chi_{3,1}(1-\cos q_{3_2}) - 2F^C_{t1,1}L_{t_{1,1}}}{2\alpha_{t_{1,1}}} \\ q_{3_{1,2}} = 0 \\ 1-\cos q_{3_2} = \dfrac{1}{4\alpha_{t_{1,1}}\alpha_{t_2} - \chi^2_{3,1}}[(2\alpha_{t_{1,1}}\beta_{t_2} + \beta_{t_{1,1}}\chi_{3,1})\sin q_1 - (2\alpha_{t_{1,1}}\chi_2 + \chi_{1,1}\chi_{3,1}) \\ \qquad \times(\ -\ \ q_2) - 2\chi_{3,1}F^C_{t1,1}L_{t_{1,1}} - 4\alpha_{t_{1,1}}F^C_{t2}L_{t_2}] \qquad 1\ \ \cos \end{cases} \tag{AII.10}$$

(xi) Uncoupled solution in $q_{3_{1,1}}$, $q_{3_{1,2}}$ and q_{3_2}

$$\begin{cases} M = \theta\sin(2q_1) - [\beta_{t_{1,1}}(1-\cos q_{3_{1,1}}) + \beta_{t_{1,2}}(1-\cos q_{3_{1,2}}) + \beta_{t_2}(1-\cos q_{3_2})]\cos q_1 \\ q_2 = 0 \\ 1-\cos q_{3_{1,1}} = \dfrac{\beta_{t_{1,1}}\sin q_1 - \chi_4(1-\cos q_{3_{1,2}}) + \chi_{3,1}(1-\cos q_{3_2}) - 2F^C_{t1,1}L_{t_{1,1}}}{2\alpha_{t_{1,1}}} \\ 1-\cos q_{3_{1,2}} = \dfrac{1}{4\alpha_{t_{1,1}}\alpha_{t_{1,2}} - \chi^2_4}([(2\alpha_{t_{1,1}}\beta_{t_{1,2}} - \beta_{t_{1,1}}\chi_4)\sin q_1 + (2\alpha_{t_{1,1}}\chi_{3,2} - \chi_{3,1}\chi_4) \\ \qquad \times(\ -\ \ q_{3_2}) + 2\chi_4 F^C_{t1,1}L_{t_{1,1}} - 4\alpha_{t_{1,1}}F^C_{t1,2}L_{t_{1,2}}] \qquad 1\ \ \cos \\ 1-\cos q_{3_2} = \dfrac{F_{11}\sin q_1 - H_{11}}{(4\alpha_{t_{1,1}}\alpha_{t_{1,2}} - \chi^2_4)(4\alpha_{t_{1,1}}\alpha_{t_2} - \chi^2_{3,1}) - (2\alpha_{t_{1,1}}\chi_{3,2} - \chi_{3,1}\chi_4)^2} \end{cases} \tag{AII.11}$$

(xii) Fully coupled solution in q_2, $q_{3_{1,1}}$, $q_{3_{1,2}}$, and q_{3_2}

$$\begin{cases} M = \theta\sin(2q_1) - [\beta_c(1-\cos q_2) + \beta_{t_{1,1}}(1-\cos q_{3_{1,1}}) + \beta_{t_{1,2}}(1-\cos q_{3_{1,2}}) + \beta_{t_2}(1-\cos q_{3_2})] \times \cos q_1 \\ A_{12}(1-\cos q_2)^3 + B_{12}(1-\cos q_2)^2 + C_{12}(1-\cos q_2) - D_{12}\sin q_1 + E_{12} = 0 \\ 1-\cos q_{3_{1,1}} = \dfrac{\beta_{t_{1,1}}\sin q_1 - \chi_{1,1}(1-\cos q_2) - \chi_4(1-\cos q_{3_{1,2}}) + \chi_{3,1}(1-\cos q_{3_2}) - 2F^C_{t1,1}L_{t_{1,1}}}{2\alpha_{t_{1,1}}} \\ 1-\cos q_{3_{1,2}} = \dfrac{1}{4\alpha_{t_{1,1}}\alpha_{t_{1,2}} - \chi^2_4}[(2\alpha_{t_{1,1}}\beta_{t_{1,2}} - \beta_{t_{1,1}}\chi_4)\sin q_1 - (2\alpha_{t_{1,1}}\chi_{1,2} - \chi_{1,1}\chi_4)(1-\cos q_2) \\ \qquad (+2\alpha_{t_{1,1}}\chi_{3,2} - \chi_{3,1}\chi_4)(1-\cos q_{3_2}) + 2\chi_4 F^C_{t1,1}L_{t_{1,1}} - 4\alpha_{t_{1,1}}F^C_{t1,2}L_{t_{1,2}}] \\ 1-\cos q_{3_2} = \dfrac{F_{12}\sin q_1 - G_{12}(1-\cos q_2) - H_{12}}{(4\alpha_{t_{1,1}}\alpha_{t_{1,2}} - \chi^2_4)(4\alpha_{t_{1,1}}\alpha_{t_2} - \chi^2_{3,1}) - (2\alpha_{t_{1,1}}\chi_{3,2} - \chi_{3,1}\chi_4)^2} \end{cases} \tag{AII.12}$$

The parameters in Eqs. (AII.1-12) are defined in Eqs. (AI.9-12) and in the Eqs. below.

$$\alpha_{c1} = 2L_c^2\left[\frac{(z_1-z_2)^2\rho}{\lambda}+k_{pc1}\right] \qquad \beta_{t_{1,j}} = \frac{2z(z_1-z_2)(z-z_2)L_{1,j}\rho}{\lambda}_{\,j=1,2}$$
$$\alpha_{t_{1,j}} = 2L_{1,j}^2\left[\frac{(z_2-z)^2\rho}{\lambda}+k_{pt_{1,j}}\right]_{j=1,2} \tag{AII.13}$$

$$\chi_{1,j} = 4L_cL_{t_{1,j}}\frac{(z_1-z_2)(z-z_2)\rho}{\lambda}_{\,j=1,2}$$

$$\chi_{3,j} = 4L_{t_{1,1}}L_{t_2}\frac{(z_1-z)(z_2-z)\rho}{\lambda}_{\,j=1,2}$$

$$\chi_4 = 4L_{t_{1,1}}L_{t_{1,2}}\frac{(z_1-z)^2\rho}{\lambda} \tag{AII.14}$$

$$\gamma_c = \frac{8}{3}L_c^3k_{pc2}$$

$$\mu_c = 4L_c^4k_{pc3} \tag{AII.15}$$

$$A_5 = 8\mu_c\alpha_{t_{1,1}} \qquad A_6 = 8\mu_c\alpha_{t_2}$$
$$B_5 = 6\gamma_c\alpha_{t_{1,1}} \qquad B_6 = 6\gamma_c\alpha_{t_2}$$
$$C_5 = 4\alpha_{c1}\alpha_{t_{1,1}}-\chi_{1,1}^2 \qquad C_6 = 4\alpha_{c1}\alpha_{t_2}-\chi_2^2$$
$$D_5 = 2\alpha_{t_{1,1}}\beta_c-\beta_{t_{1,1}}\chi_{1,1} \qquad D_6 = 2\alpha_{t_2}\beta_c-\beta_{t_2}\chi_2$$
$$E_5 = 4\alpha_{t_{1,1}}F_c^CL_c-2\chi_{1,1}F_{t1,1}^CL_{t_{1,1}} \qquad E_6 = 4\alpha_{t_2}F_c^CL_c-2\chi_2F_{t2}^CL_{t_2} \tag{AII.16}$$

$$A_9 = A_5(4\alpha_{t_{1,1}}\alpha_{t_{1,2}}-\chi_4^2)$$

$$B_9 = B_5(4\alpha_{t_{1,1}}\alpha_{t_{1,2}}-\chi_4^2)$$

$$C_9 = C_5(4\alpha_{t_{1,1}}\alpha_{t_{1,2}}-\chi_4^2)-(2\alpha_{t_{1,1}}\chi_{1,2}-\chi_{1,1}\chi_4)^2$$

$$D_9 = D_5(4\alpha_{t_{1,1}}\alpha_{t_{1,2}}-\chi_4^2)-(2\alpha_{t_{1,1}}\chi_{1,2}-\chi_{1,1}\chi_4)(2\alpha_{t_{1,1}}\beta_{t_{1,2}}-\beta_{t_{1,1}}\chi_4)$$

$$E_9 = 4\alpha_{t_{1,1}}[(4\alpha_{t_{1,1}}\alpha_{t_{1,2}}-\chi_4^2)F_c^CL_c-(2\alpha_{t_{1,2}}\chi_{1,1}-\chi_{1,2}\chi_4)F_{t1,1}^CL_{t_{1,1}}-(2\alpha_{t_{1,1}}\chi_{1,2}-\chi_{1,1}\chi_4)F_{t1,2}^CL_{t_{1,2}}] \tag{AII.17}$$

$$A_{10} = A_5(4\alpha_{t_{1,1}}\alpha_{t_2}-\chi_{3,1}^2)$$

$$B_{10} = B_5(4\alpha_{t_{1,1}}\alpha_{t_2}-\chi_{3,1}^2)$$

$$C_{10} = C_5(4\alpha_{t_{1,1}}\alpha_{t_2}-\chi_{3,1}^2)-(2\alpha_{t_{1,1}}\chi_2+\chi_{1,1}\chi_{3,1})^2$$

$$D_{10} = D_5(4\alpha_{t_{1,1}}\alpha_{t_2} - \chi_{3,1}^2) - (2\alpha_{t_{1,1}}\chi_2 + \chi_{1,1}\chi_{3,1})(2\alpha_{t_{1,1}}\beta_{t_2} + \beta_{t_{1,1}}\chi_{3,1})$$

$$E_{10} = 4\alpha_{t_{1,1}}[(4\alpha_{t_{1,1}}\alpha_{t_2} - \chi_{3,1}^2)F_c^C L_c - (2\alpha_{t_2}\chi_{1,1} + \chi_2\chi_{3,1})F_{t1,1}^C L_{t_{1,1}} - (2\alpha_{t_{1,1}}\chi_2 + \chi_{1,1}\chi_{3,1})F_{t2}^C L_{t_2}] \quad \text{(AII.18)}$$

$$F_{11} = (4\alpha_{t_{1,1}}\alpha_{t_{1,2}} - \chi_4^2)(2\alpha_{t_{1,1}}\beta_{t_2} + \beta_{t_{1,1}}\chi_{3,1}) + (2\alpha_{t_{1,1}}\chi_{3,2} - \chi_{3,1}\chi_4)(2\alpha_{t_{1,1}}\beta_{t_{1,2}} - \beta_{t_{1,1}}\chi_4)$$

$$H_{11} = 4\alpha_{t_{1,1}}[(2\alpha_{t_{1,2}}\chi_{t_{3,1}} - \chi_{3,2}\chi_4)F_{t1,1}^C L_{t_{1,1}} + (2\alpha_{t_{1,1}}\chi_{3,2} - \chi_{3,1}\chi_4)F_{t1,2}^C L_{t_{1,2}} + (4\alpha_{t_{1,1}}\alpha_{t_{1,2}} - \chi_4^2)F_{t2}^C L_{t_2}] \quad \text{(AII.19)}$$

$$A_{12} = A_9[(4\alpha_{t_{1,1}}\alpha_{t_{1,2}} - \chi_4^2)(4\alpha_{t_{1,1}}\alpha_{t_2} - \chi_{3,1}^2) - (2\alpha_{t_{1,1}}\chi_{3,2} - \chi_{3,1}\chi_4)^2]$$

$$B_{12} = B_9[(4\alpha_{t_{1,1}}\alpha_{t_{1,2}} - \chi_4^2)(4\alpha_{t_{1,1}}\alpha_{t_2} - \chi_{3,1}^2) - (2\alpha_{t_{1,1}}\chi_{3,2} - \chi_{3,1}\chi_4)^2]$$

$$C_{12} = C_9[(4\alpha_{t_{1,1}}\alpha_{t_{1,2}} - \chi_4^2)(4\alpha_{t_{1,1}}\alpha_{t_2} - \chi_{3,1}^2) - (2\alpha_{t_{1,1}}\chi_{3,2} - \chi_{3,1}\chi_4)^2] - G_{12}^2$$

$$D_{12} = D_9[(4\alpha_{t_{1,1}}\alpha_{t_{1,2}} - \chi_4^2)(4\alpha_{t_{1,1}}\alpha_{t_2} - \chi_{3,1}^2) - (2\alpha_{t_{1,1}}\chi_{3,2} - \chi_{3,1}\chi_4)^2] - G_{12}F_{12}$$

$$E_{12} = E_9[(4\alpha_{t_{1,1}}\alpha_{t_{1,2}} - \chi_4^2)(4\alpha_{t_{1,1}}\alpha_{t_2} - \chi_{3,1}^2) - (2\alpha_{t_{1,1}}\chi_{3,2} - \chi_{3,1}\chi_4)^2] - G_{12}H_{12}$$

$$F_{12} = F_{11}$$

$$G_{12} = (4\alpha_{t_{1,1}}\alpha_{t_{1,2}} - \chi_4^2)(2\alpha_{t_{1,1}}\chi_2 - \chi_{1,1}\chi_{3,1}) + (2\alpha_{t_{1,1}}\chi_{1,2} - \chi_{1,1}\chi_4)(2\alpha_{t_{1,1}}\chi_{3,2} - \chi_{3,1}\chi_4)$$

$$H_{12} = H_{11} \quad \text{(AII.20)}$$

DN